Atomic and electronic structure of the Si(001)-Rb chemisorption system at 0.5 and 1.0 monolayer coverage

H. Q. Shi, M. W. Radny, and P. V. Smith*

School of Mathematical and Physical Sciences, The University of Newcastle, Callaghan, Australia 2308

(Received 23 October 2003; revised manuscript received 9 September 2004; published 9 February 2005)

The atomic and electronic structure of the Si(001)-Rb chemisorption system at 0.5 and 1.0 monolayer coverage has been investigated using the plane wave, pseudopotential density functional method contained in the VASP code. The atomic and electronic structures of the Rb chemisorption system at 0.5 monolayer coverage are found to be very similar to the Li chemisorption system at the same coverage. The minimum energy structure determined for the Si(001)-Rb chemisorption system at 1.0 ML coverage has been found to be in good agreement with the x-ray standing-wave (XSW) field data. The predicted occupied and unoccupied electronic surface state bands have also been shown to be in excellent agreement with the ARUPS and IPES results. The calculations suggest that the bonding between the Rb adatoms and the Si substrate atoms is neither purely ionic nor covalent. No evidence has been found in support of strong Rb-Rb interactions and the formation of a metallic overlayer.

I. INTRODUCTION

The chemisorption of alkali metals (AM) on the (001) surface of silicon has been widely studied.[1–3] In order to elucidate trends resulting from such interactions it is important to possess data for all of the elements of a given group of the periodic table. Of the Group I elements, the interaction of potassium and sodium with the Si(001) surface has been fairly well studied both theoretically and experimentally.[4–12] Recently, we have performed detailed calculations of the atomic and electronic structure of the Si(001)-Li chemisorption system,[13] and compared the results of these calculations with the existing experimental data,[14–24] and earlier theoretical work.[10,25,26] While some experimental work has been published on the interaction of Rb with the Si(001) surface,[29–33] no theoretical investigation of this Si(001)-AM chemisorption system has been reported to our knowledge. The aim of this paper is to report the results of *ab initio* calculations of the atomic and electronic structure of the Si(001)-Rb system at 0.5 and 1.0 monolayer (ML) coverage.

X-ray standing-wave field (XSW) experiments were performed by Eteläniemi *et al.*[27] to investigate the atomic structure of the Si(001)2×1-Rb adsorption system. At room temperature (RT), for one monolayer (1.0 ML) coverage, the Rb atoms were predicted to sit at the pedestal and valley bridge sites [these sites are labeled Rb(*A*) and Rb(*C*) in Figs. 1(c) and 1(d)]. This *AC* structure is identical to the so-called double layer (DL) model that had been proposed for the atomic structure of the Si(001)2×1-K adsorption system at 1.0 ML coverage by Abukawa and Kono.[6] From their data analysis, Eteläniemi *et al.*[27] concluded that a symmetric dimer structure is energetically favored at 1.0 ML coverage, with the dimer length being 2.3–2.4 Å. Chao *et al.*[28] used photoelectron spectroscopy to study the adsorption of Rb on the Si(001)2×1 surface at RT for increasing Rb coverage. They observed two components in the Rb 4*p* and 3*d* spectra at coverages higher than ∼2/3 ML. This indicated the presence of two different Rb adsorption sites, in support of the

DL model. At saturation coverage (∼1.0 ML) they found the LEED data exhibited a 2×1 periodicity which they believed was due to the underlying Si dimer reconstruction. Castrucci *et al.*[29] used the XSW method to study Rb adsorption on the Si(001)2×1 surface at low (0.19±0.02 ML) coverage and determined the Rb-Si bond length to be 3.06±0.03 Å.

Angle-resolved photoemission (ARUPS) has been used to study the electronic structure of the Si(001)2×1-Rb system at RT by Chao *et al.*[30] At saturation coverage two occupied surface states separated by ∼1.0 eV were found at normal emission [this corresponds to the Γ point of the Surface Brillouin zone (SBZ)]. The dispersions of these two surface state bands were also determined by these authors along the [010] direction at saturation coverage. This direction corresponds to the Γ-J_2' symmetry direction in the SBZ [see Fig. 1(b)]. A third surface state band was also observed along this Γ-J_2' direction.

Both angle-resolved direct (ARUPS) and inverse (IPES) photoemission have been used by Johansson *et al.*[31] to study the development of the surface electronic structure of a rubidium-adsorbed Si(001)2×1 surface with increasing Rb coverage. Emission from the Si empty dangling-bond surface state was observed for Rb coverages up to around 0.5 ML. A new surface-related structure was also found to appear in the IPES spectra for the Γ point with an energy of 1.5 eV above the Fermi energy at a coverage of around 1/3 ML. The energy of this structure was observed to shift downward with further increasing coverage and at saturation coverage (∼1.0 ML) was 0.25 eV above the Fermi energy. The dispersion of this unoccupied surface state band was recorded along the [011] and [01$\bar{1}$] orientations for saturation coverage; that is, along the Γ-J' and Γ-J symmetry directions of the SBZ [see Fig. 1(b)]. Parabolic-like shapes with large dispersions of up to 1.4 eV were observed along both directions. Johansson *et al.*[31] concluded that this surface state band was derived from a Rb-overlayer state with strong Rb $5p_z$ character, and that its large parabolic dispersion results from strong Rb-Rb interactions within the metallic overlayer in
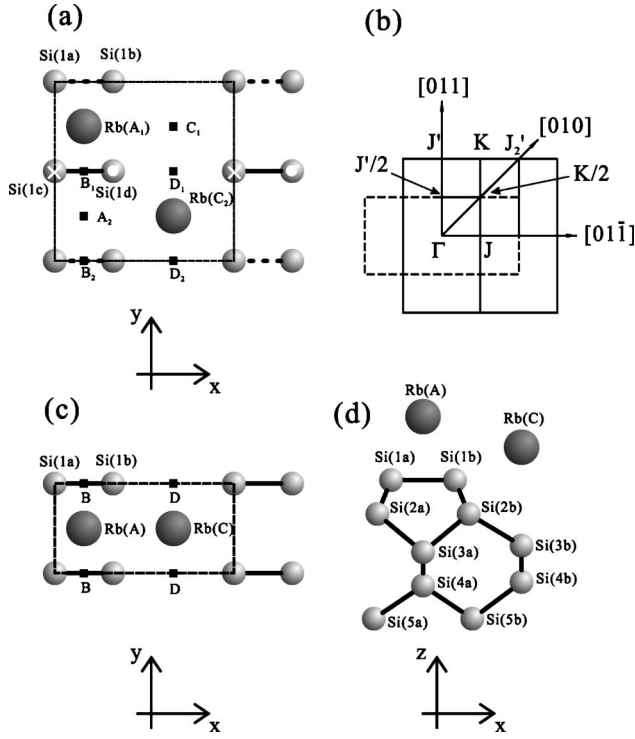
FIG. 1. (a) Top view of our minimum energy configuration for the Si(001)2×2-Rb chemisorption system at 0.5 ML coverage. The dashed lines denote the 2×2 SUC. The upper and lower rubidium atoms which lie close to the pedestal and valley bridge sites are denoted by the symbols Rb(A_1) and Rb(C_2), respectively. The dimer bridge and cave sites are indicated by the symbols B_1, B_2 and D_1 and D_2, respectively. The dimer indicated by the dashed line is almost flat while the dimer denoted by the solid line is buckled with the ○ and × indicating the up and down atoms, respectively. The SBZ of the (2×1) and (2×2) SUC are shown in (b). Top and side views of our minimum energy configuration for the Si(001)2×1-Rb chemisorption system at 1.0 ML coverage are shown in (c) and (d). The dashed lines in (c) denote the 2×1 SUC. The upper and lower rubidium atoms at the pedestal and valley bridge sites are denoted in (c) and (d) by the symbols Rb(A) and Rb(C), respectively. The dimer bridge and cave sites are indicated by the symbols B and D.

both the [011] and [01$\bar{1}$] directions. They also found that the surface electronic structure at 1.0 ML Rb coverage was semiconducting with a surface band gap of ~0.6 eV.

Despite all of the above experimental work, several aspects concerning the basic properties of the Si(001)2×1-Rb chemisorption system require further investigation. These include the actual chemisorption sites of the rubidium atoms, the nature of the Rb-Si bonds, and the degree of metallization of the system as a function of coverage. A detailed investigation of the properties of Rb adsorption on the Si(001) surface would also be helpful in providing an overall understanding of Si(001)-AM adsorption systems. In this paper, we report the results of accurate first-principles calculations of the atomic and electronic structure of the Si(001)2×1-Rb system at 0.5 and 1.0 ML coverage, and compare these results with the currently available experimental data.

II. METHOD AND PROCEDURE

All of the calculations reported in this paper have been carried out using the *ab initio* total-energy and molecular dynamics program VASP (Vienna *ab initio* simulation package) which is based on the density functional theory (DFT) pseudopotential plane wave method.[32–34] The calculations have been performed using both the PAW potentials[35,36] and the Ultra-Soft (US) Vanderbilt pseudopotentials[37] included in the VASP code.[32–34] In the PAW potential of rubidium both the s and p semi-core states were treated as valence states. The Ceperley-Alder local density approximation (LDA) exchange and correlation functional has been employed for both sets of the potentials. The Kohn-Sham equations were solved using 4 special k points in the irreducible symmetry element of the SBZ of the Si(001)2×1 and 2×2 surface unit cells (SUC), and employing plane waves with kinetic energies up to ~20 Rydbergs. For our 2×1 and 2×2 periodic unit cells we have employed 8 layers of silicon plus 4 and 8 hydrogen atoms, respectively, to saturate the dangling bonds of the bottom layer silicon atoms, and a vacuum region of ~12 Å. The minimum energy structures were determined by minimizing the forces using the Hellmann-Feynman theorem and allowing all of the coordinates of the silicon atoms in the top four layers of the slab, plus those of the chemisorbed rubidium atoms, to vary. To identify the electronic surface states we have calculated the function $\rho_{nk}(z)$ defined by

$$\rho_{nk}(z) = \int_{SUC} |\Psi_{nk}(x,y,z)|^2 dxdy,$$

where x and y lie in the surface plane, z is out of the surface, and the integration is performed over the SUC. The silicon dimer atoms in our 8 layer slab are sited at $z \sim 0$ Å while the terminating hydrogen atoms are at $z \sim -10.3$ Å. Three-dimensional (3D) charge distributions were also calculated for all of the identified electronic surface states in order to unambiguously determine the nature of the individual surface state bands. To simplify the 3D pictures, these latter calculations were realized using the US pseudopotentials.

III. RESULTS

A. Atomic structure

1. Si(001)2×2-Rb system at 0.5 ML coverage

In order to determine the minimum energy structure of the Si(001)2×2-Rb system at 0.5 ML coverage, we carried out geometry optimization calculations for six different starting geometries [A_2C_2, A_1C_2, B_1C_2, A_1A_2, A_1D_2, and C_1C_2—see Fig. 1(a)]. The calculations for three of these initial geometries (A_1C_2, A_1D_2, and B_1C_2) converged to the same optimized geometry, the A_1C_2 configuration. This A_1C_2 configuration, in which the optimized position of A_1 is displaced along the positive x axis from the pedestal site by 0.13 Å, is the most energetically favorable structure. Energy values for the four different stable structures that we have determined are presented in Table I. The atomic relaxations, and various bond lengths of interest for the A_1C_2 configuration, are presented in Table II.

TABLE I. The energies (in eV) of the different atomic configurations of the Si(001)2×2-Rb chemisorption system for 0.5 ML coverage, relative to that of the lowest energy configuration. The notation for the various sites is the same as that in Fig. 1(a).

Configuration	Energy
A_1C_2	0.00
C_1C_2	0.096
A_2C_2	0.277
A_1A_2	0.679

The structures of the silicon substrate for the four stable optimized configurations that we obtained were found to be nearly identical. This substrate structure, which has one buckled and one flat dimer, is very similar to that of the Si(001)2×2-Li chemisorption system at 0.5 ML coverage (see Ref. 13). The buckling angle of the buckled dimer of 6.1°, however, is considerably flatter than that of the Si(001)2×2-Li chemisorption system (14.5°). The bond length of this dimer of 2.25 Å is also somewhat shorter than the corresponding bond length of 2.32 Å in the Si(001)2×2-Li system. The bond length of the flat dimer, which has a buckling angle of only 0.3°, is 2.47 Å. This is the same as the bond length of the corresponding dimer in the Si(001)2×2-Li system at 0.5 ML coverage, which has a buckling angle of 3.2°.

The adatom topologies of the Si(001)2×2-Rb and Si(001)2×2-Li minimum energy configurations at 0.5 ML coverage also show some differences with the former having the two adatoms near A and C sites, while the latter system

TABLE II. Optimized geometry (in Å) of the Si(001)2×2-Rb chemisorption system at 0.5 ML coverage for the minimum energy A_1C_2 structure. Δz is the vertical displacement relative to the ideal bulk terminated surface, and d denotes the various bond lengths in Å. The labeling of the atoms is the same as in Fig. 1(a).

	Value (Å)
$\Delta z_{Rb(A1)}$	2.37
$\Delta z_{Rb(C2)}$	1.36
$\Delta z_{Si(1a)}$	0.10
$\Delta z_{Si(1b)}$	0.08
$\Delta z_{Si(1c)}$	−0.65
$\Delta z_{Si(1d)}$	−0.08
$d_{Si(1a)\text{-}Si(1b)}$	2.47
$d_{Si(1c)\text{-}Si(1d)}$	2.25
$d_{Si(1a)\text{-}Rb(A1)}$	3.27
$d_{Si(1b)\text{-}Rb(A1)}$	3.23
$d_{Si(1c)\text{-}Rb(A1)}$	3.71
$d_{Si(1d)\text{-}Rb(A1)}$	3.34
$d_{Si(1a)\text{-}Rb(C2)}$	3.43
$d_{Si(1b)\text{-}Rb(C2)}$	3.37
$d_{Si(1c)\text{-}Rb(C2)}$	4.04
$d_{Si(1d)\text{-}Rb(C2)}$	3.48

TABLE III. Total energies of the different structures of the Si(001)2×1-Rb system at monolayer coverage relative to that of the minimum energy AC structure.

Configuration	Energy (eV)	
	US	PAW
AC	0.00	0.00
BC	0.42	0.45
AD	0.57	0.58
BD	1.01	1.07

prefers the Li adatoms to reside close to the A and D sites.[13] In the early studies of AM-Si(001) chemisorption systems it was assumed that Levine's model[4] for Cs adsorption on the Si(001) surface would be valid for all of the AM's at 0.5 ML coverage. In this model, the adatoms were assumed to be chemisorbed at the pedestal sites along the hills of the dimer rows [the A site in Fig. 1(c)]. Levine's model, however, is predicted by our calculations to be the highest energy structure for the Si(001)2×2-Rb system at 0.5 ML coverage (see structure A_1A_2 in Table I). Unfortunately, no experimental data on the atomic structure of the Si(001)-Rb chemisorption system at 0.5 ML coverage are available for comparison with our theoretical results.

2. Si(001)2×1-Rb system at 1.0 ML coverage

In order to determine the minimum energy structure of the Si(001)2×1-Rb system at monolayer coverage, geometry optimization calculations were carried out for four different starting geometries. These were the AC, AD, BC, and BD configurations [see Fig. 1(c)]. Calculations were performed for these four structures using both a 2×1 and 2×2 SUC. In some of the 2×2 calculations different starting values were assigned to the z coordinates of each of the Rb adatoms. Despite this additional flexibility, these calculations always resulted in a 2×1 periodicity. This suggests that interactions between the dimers do not play a significant role in determining the atomic structure. The relative energies of these four structures obtained using both the US pseudopotentials and PAW potentials are presented in Table III. The DL model structure, in which the two rubidium atoms sit at the pedestal (A) and valley bridge (C) sites [see Figs. 1(c) and 1(d)], is found to be the most stable. This is consistent with the results of Eteläniemi *et al.* who found that the DL model provided the best fit to their XSW results.[27] The atomic relaxations and various bond lengths of interest obtained from both our PAW and US optimized geometries and the XSW experiments, are presented in Table IV. The PAW and US values are seen to agree very closely. In all of the following text we thus only discuss the PAW results. The Si-Si dimers were predicted by our calculations to be completely symmetrical. This agrees with the XSW results[27] which indicated identical vertical displacements of −0.2 Å for each pair of Si dimer atoms from their ideal bulk values. The calculated dimer length of 2.49 Å is also in reasonable agreement with the XSW value of 2.3–2.4 Å.[27] Our calculated bond length be-

TABLE IV. Optimized geometry (in Å) of the Si(001)2×1-Rb system at 1.0 ML coverage obtained using the VASP code with PAW potentials and US pseudopotentials, compared with the experimental results of Eteläniemi *et al.* (Ref. 27). Δz is the vertical displacement relative to the ideal bulk terminated surface, and d denotes the various bond lengths in Å. The labeling of the atoms is the same as in Fig. 1(c).

	This work PAW (US)	Ref. 27
$\Delta z_{Rb(A)}$	2.42 (2.42)	
$\Delta z_{Rb(C)}$	1.23 (1.24)	
$\Delta z_{Rb(A)}$-$\Delta z_{Rb(C)}$	1.19 (1.18)	0.8±0.2
$\Delta z_{Si(1a)}$	0.00 (−0.03)	−0.2
$\Delta z_{Si(1b)}$	0.00 (−0.03)	−0.2
$d_{Si(1a)-Si(1b)}$	2.49 (2.48)	2.3−2.4
$d_{Si(1a)-Rb(A)}$	3.32 (3.35)	
$d_{Si(1b)-Rb(A)}$	3.32 (3.35)	
$d_{Si(1a)-Rb(C)}$	3.43 (3.45)	3.31±0.1
$d_{Si(1b)-Rb(C)}$	3.43 (3.45)	

tween the silicon dimer atoms and the upper rubidium atom [Rb(A)] is 3.32 Å, while the bond length between the silicon dimer atoms and the lower rubidium atom [Rb(C)] is 3.43 Å. These values correlate well with the value of 3.31 Å used by Eteläniemi *et al.*[27] to fit their XSW data at 1.0 ML coverage. These authors also determined the vertical distance between the rubidium atoms sitting at the valley and pedestal sites to be 0.8±0.2 Å. The corresponding value derived from our VASP calculations is significantly greater at 1.19 Å.

B. Electronic structure

1. Si(001)2×2-Rb system at 0.5 ML coverage

Electronic structure calculations have been carried out for our minimum energy Si(001)2×2-Rb configuration at 0.5 ML coverage. The resulting eigenenergies in the vicinity of the energy gap have been determined for 80 k-points along the Γ-J-$K/2$-$J'/2$-Γ symmetry directions of the 2×2 SBZ and the resulting energy bands plotted in Fig. 2(a). We observe that the band structure of the Si(001)2×2-Rb system at 0.5 ML coverage is very similar to the band structure of the Si(001)2×2-Li system at 0.5 ML coverage [see Fig. 3(a) in Ref. 13]. This includes the whole of the valence band structure as well as the dispersion of the band corresponding to the lowest unoccupied molecular orbital (LUMO). The similarity of the two valence band structures is consistent with the almost identical Si(001)2×2 substrate reconstructions induced by the Rb and Li adatoms. The overall similarity of the two band structures also suggests that the nature of the surface states of the Si(001)2×2-Rb system at 0.5 ML coverage will be analogous to that of the 0.5 ML Si(001)2×2-Li chemisorption system [see Fig. 3(b) in Ref. 13]. The LUMO band of the Si(001)2×2-Li system at 0.5 ML coverage has been identified as the π^* surface state band associated with the asymmetric silicon dimers. Johansson *et al.*[31] found that normal emission from the empty
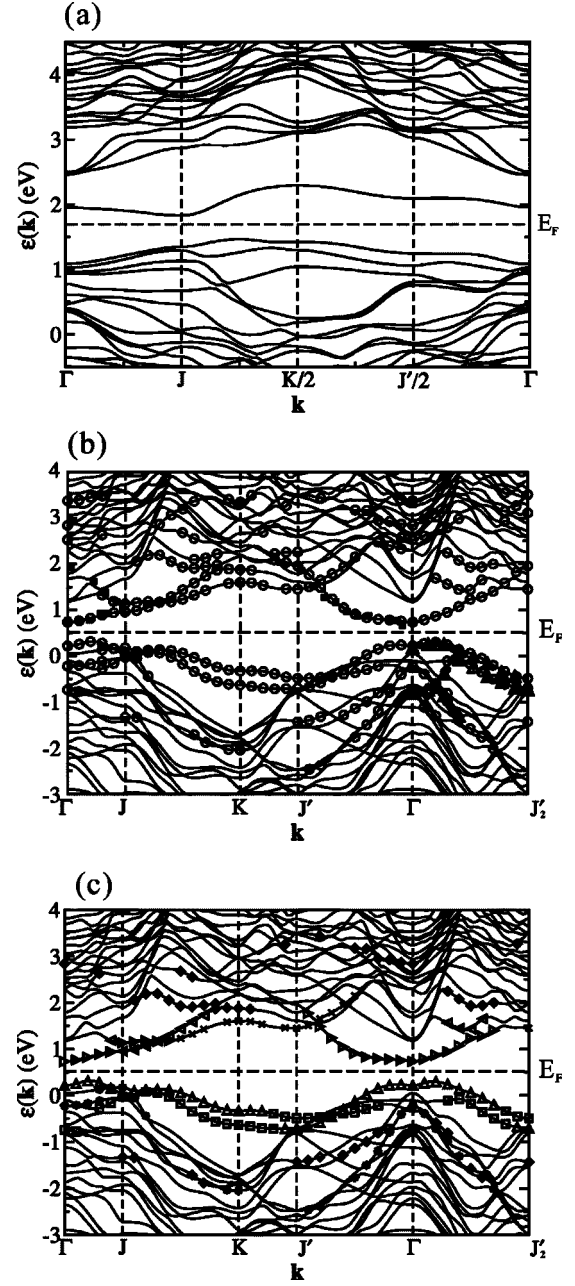

FIG. 2. (a) Surface electronic structure of the Si(001)2×2-Rb chemisorption system at 0.5 ML coverage in the vicinity of the Fermi energy. (b) Electronic structure of the Si(001)2×1-Rb system at 1.0 ML coverage in the vicinity of the Fermi energy. The empty circles indicate the theoretically predicted surface states. The filled circles and empty triangles denote the ARUPS data of Chao *et al.* (Ref. 30) while the filled squares represent the IPES data of Johansson *et al.* (Ref. 31). (c) The different character of the electronic surface states identified by the theoretical calculations. Occupied states: $\triangle$ π^* Si dangling bond surface state, $\square$ π Si dangling bond surface state, $\diamond$ Si dimer σ bond surface state, $*$ first silicon back bond state. Unoccupied states: $\triangleright$ π Si dangling bond plus upper Rb orbitals, $\triangleleft$ π^* Si dangling bond plus lower Rb orbitals, $\times$ upper Rb and subsurface Si orbitals, $\blacklozenge$ anti-bonding σ^* Si dimer bond plus lower Rb orbitals.

dangling-bond surface state (labeled U_1 in Ref. 31) is visible up to a Rb coverage corresponding to a work function of −2.75 eV. They also found that a work function of −1.98 eV corresponded to 1/3 ML coverage while a work function of around −3.50 eV matched to 1.0 ML coverage. Taking these values as our reference, we estimate that the lowest energy unoccupied π^* surface state of the Si(001)2×2-Rb system at 0.5 ML coverage at the Γ point of the SBZ should be located about 0.6 eV above the Fermi energy. Our theoretically predicted LUMO π^* surface state band for the Si(001)2×2-Rb system at 0.5 ML coverage is predicted to lie 0.27 eV above the Fermi energy at the Γ point.

2. Si(001)2×1-Rb system at 1.0 ML coverage

Electronic structure calculations have been carried out for our minimum energy Si(001)2×1-Rb DL model structure at 1.0 ML coverage. The resulting eigenenergies in the vicinity of the energy gap have been determined for 160 $\boldsymbol{k}$-points along the Γ-J-K-J'-Γ-J'_2 symmetry directions of the SBZ and the resulting energy bands plotted in Fig. 2(b). In order to identify the electronic surface states, the function $\rho_{nk}(z)$ has been calculated at 40 $\boldsymbol{k}$-points along these symmetry directions for all the bands within several eV of the Fermi energy. The identified surface states are indicated in Fig. 2(b) by the empty circles. The ARUPS data for the occupied surface states obtained by Chao et al.[30] for the Si(001)2×1-Rb system at 1.0 ML coverage in the vicinity of the Fermi energy is also shown in Fig. 2(b) (filled circles and empty triangles). The data indicated by the filled circles were obtained from a surface prepared by Rb deposition directly onto a cold Si(001)c(4×2) surface, while the data indicated by the empty triangles are for a surface cooled after preparation at room temperature (RT). The IPES data for the unoccupied surface states obtained by Johansson et al.[31] in the vicinity of the Fermi energy for the Si(001)2×1-Rb system at ∼1.0 ML coverage is also presented in Fig. 2(b). This data is indicated by the filled squares. The ARUPS data[30] has been shifted up by 0.21 eV to match the theoretically predicted values close to the Γ point. The IPES data[31] have been left unchanged.

As can be seen from Fig. 2(b), there is excellent agreement between the theoretical results and the experimental data for both the occupied and unoccupied states. The ARUPS data of Chao et al.[30] predicted the occurrence of two occupied surface states at the Γ point of the SBZ with an energy separation of ∼1.0 eV. Our calculations also predict two surface states with a calculated energy separation at the Γ point of 0.95 eV. The lower of the two experimental surface state bands is observed to initially disperse upward along the Γ-J' symmetric direction, while the upper surface state band remains fairly flat. Once the two bands almost meet, however, midway along the Γ-J'_2 symmetry direction, they both disperse downward with similar dispersion before becoming essentially degenerate close to the J'_2 symmetry point. Our calculated results are seen to correlate extremely well with the experimental data for these two surface state bands. The surface states at the J'_2 symmetry point are determined from the ARUPS experiments to lie ∼0.95 eV lower

than the highest occupied surface state at the Γ point. The energy difference between these states predicted by our calculations is 0.92 eV, in excellent agreement with the ARUPS result. The ARUPS experiments of Chao et al.[30] also discovered a third occupied surface state band that dispersed strongly downward along Γ-J'_2 [see Fig. 2(b)]. We observe that the theoretical calculations predict two surface state bands in this region with similar downward dispersion.

The IPES experiments by Johannson et al.[31] have evidenced an unoccupied surface state band that disperses upward along the Γ-J and Γ-J' symmetric directions of the SBZ. The theoretical calculations are observed to accurately reproduce this unoccupied surface state band, with the predicted dispersions being in excellent agreement with the IPES data. The IPES experiments also determined a second unoccupied surface state along the Γ-J symmetric direction that disperses strongly upwards from the J point. Our theoretical calculations also predict a second surface state near the J point with an upward dispersion.

C. Nature of the surface states of the Si(001)2×1-Rb system at 1.0 ML coverage

In order to understand the nature of the occupied and unoccupied surface states of the Si(001)2×1-Rb system at 1.0 ML coverage, we have calculated the $\rho_{nk}(z)$ function, along with the charge/probability density, for all of the theoretically predicted surface states. The varying character of these states is indicated by the use of different symbols in Fig. 2(c).

The occupied electronic surface states denoted by the empty triangles and squares in Fig. 2(c) represent the silicon dangling bond surface states. Three-dimensional (3D) charge density plots for these surface states at the K point of the SBZ are presented in Figs. 3(a) and 3(b), together with the corresponding $\rho_{nk}(z)$. The band denoted by the squares represents the π silicon dangling bond surface state [Fig. 3(a)], while the band denoted by the triangles corresponds to the π^* Si dangling bond surface state [Fig. 3(b)]. In both cases, the charge distribution is seen to be localized in the vicinity of the silicon surface dimer atoms (i.e., around z=0 Å). On the Si(001) clean surface, the π^* orbitals are usually unoccupied. For the Si(001)2×1-Rb system at 1.0 ML coverage, however, the energies of these orbitals are pushed below the Fermi level. This suggests that a significant amount of electronic charge is transferred from the Rb adatoms to the Si dimers and that ionic Rb-Si bonds are formed. As a result, the π^* orbitals become occupied and the Si(001)2×1 asymmetric dimer surface is reconstructed to the symmetric dimer (2×1) surface. Analysis of the composition of these predominantly Si π and π^* molecular orbitals also shows significant contributions from the Rb atomic orbitals. Such contributions are clearly seen in the charge density plots for the π and π^* surface state bands at the J point of the SBZ presented in Figs. 3(c) and 3(d), respectively. Detailed analysis of the molecular orbitals for the states shown in Figs. 3(a) and 3(c) reveals that they can be regarded as combinations of the π Si dangling bond orbitals and contributions from the lower and upper rubidium atoms, respectively. Similarly, the
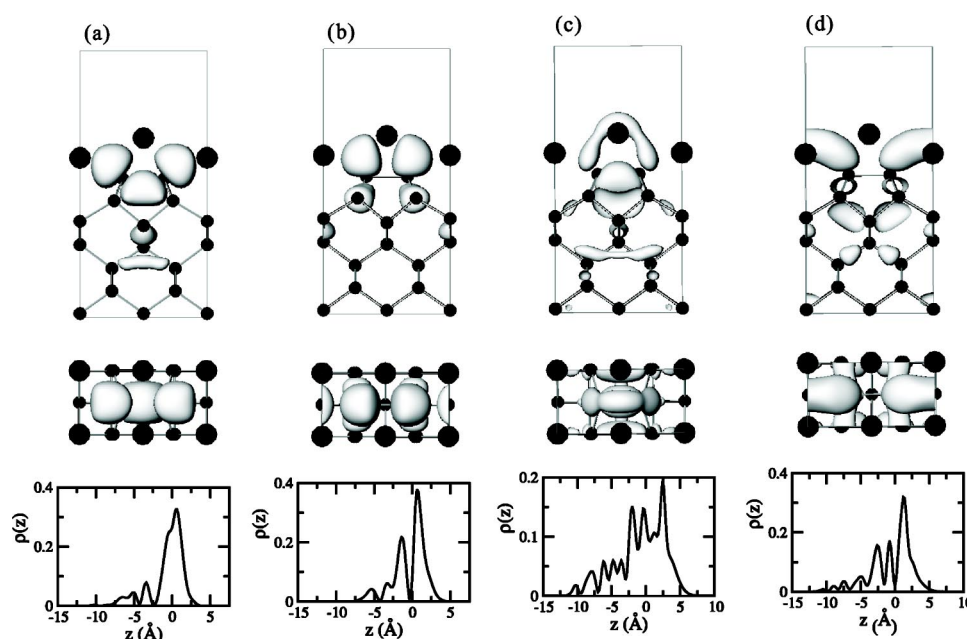
FIG. 3. Side and top views of the 3D charge density distribution, and the corresponding $\rho_{nk}(z)$, for the valence band surface states of the Si(001)2×1-Rb system at 1.0 ML coverage indicated in Fig. 2(c) by the squares [(a) and (c)] and the triangles [(b) and (d)]. The plots in (a) and (b) are for the K-point and those in (c) and (d) are for the J-point. The charge density isosurface value in each case was 0.8 ×10^{-2} e/Å^3. In this figure, and all subsequent figures, the larger and smaller filled circles represent the rubidium and silicon atoms, respectively, and the silicon dimer is centered within the 2×1 SUC, as shown in the top view. The silicon dimer atoms are sited at z ~0 Å and the hydrogen atoms on the bottom are at z ~ −10.3 Å.

molecular orbitals for the states shown in Figs. 3(b) and 3(d) can be regarded as combinations of the π^* Si dangling bond orbitals and contributions from the upper and lower rubidium atoms, respectively. Using the definition by Coulson *et al.*,[38] we have calculated the ionicity of the bonds between the upper Rb atom and the Si dimer atoms [Rb(A)-Si], and between the lower Rb atom and the Si dimer atoms [Rb(C)-Si]. The resulting values were 0.52 and 0.48, respectively. These values indicate that the bonding structure of the Rb/Si(001) chemisorption system is neither purely ionic nor purely covalent, but rather of an ionic-covalent nature.

The significant contribution of covalent bonding to the Rb/Si(001) chemisorption system suggests that there might be significant distortions in the dispersion of the π and π^* surface state bands in comparison with those of the clean surface. In order to confirm this prediction we calculated the surface electronic band structure of the substrate of the 1.0 ML Si(001)2×1-Rb system by removing the Rb atoms from the chemisorbed surface, but leaving all of the silicon atom positions unchanged. The resulting energy bands in the vicinity of the energy gap are indicated by the continuous lines in Fig. 4. The occupied π and π^* Si dangling bond molecular orbitals of the Si(001)2×1-Rb system at 1.0 ML coverage are also shown in Fig. 4 (as indicated by the symbols). Filled symbols indicate surface states which have a significant contribution from the upper rubidium atom [Rb(A)], while empty symbols indicate surface states for which the lower rubidium atom [Rb(C)] makes an important contribution. Surface states with comparable contributions from both rubidium atoms are denoted by symbols containing both black and white. Comparing the π and π^* surface

states of the chemisorbed surface with the electronic structure of the clean Si(001) substrate, we observe that the π and π^* surface states associated with the upper Rb atom [Rb(A)]
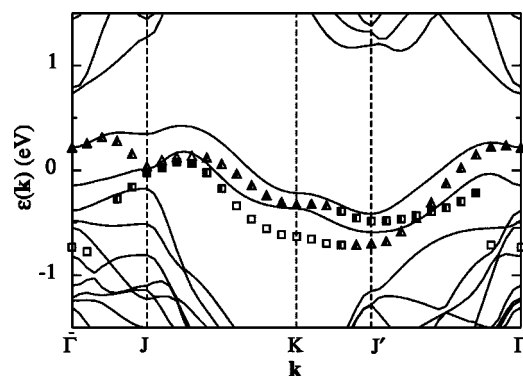

FIG. 4. Electronic structure of the substrate of the Si(001)2 ×1-Rb system at 1.0 ML coverage in the vicinity of the Fermi energy. The continuous lines indicate the energy bands for the re-constructed clean Si(001) substrate while the squares and triangles denote the occupied π and π^* surface states, respectively, for the Si(001)2×1-Rb system at 1.0 ML coverage. Filled symbols indicate surface states whose contribution from the upper rubidium atom [Rb(A)] is at least twice that from the lower rubidium atom [Rb(C)], while empty symbols indicate surface states for which the lower rubidium atom makes a contribution at least twice that of the upper rubidium atom. Surface states with similar contributions from both rubidium atoms are denoted by symbols which are both black and white. The energy bands of the substrate have been shifted downward to match the calculated Si(001)2×1-Rb results at the Γ point of the SBZ.

(filled symbols in Fig. 4) have quite similar dispersion to the corresponding surface state bands of the clean reconstructed substrate. The dispersion of the occupied surface states associated with the lower Rb atom (empty symbols in Fig. 4), on the other hand, differ significantly from those of the clean substrate. The effect of the lower Rb adatom on the dispersion of the surface state bands is clearly seen in the vicinity of the high symmetry points of the SBZ. Near the J and J' symmetry points the π^* band for the chemisorbed surface deviates significantly from that of the clean reconstructed substrate while the π band follows the dispersion of the clean substrate. In the vicinity of the K and Γ symmetry points the situation reverses—the π^* band follows the dispersion of the reconstructed clean Si(001) surface while the π band deviates significantly from that of the clean substrate. The most drastic changes in the dispersion of the surface bands are observed near the Γ point along the J-Γ and J'-Γ symmetry directions where the π band for the chemisorbed surface disperses strongly downward. This behavior is very different from that observed for the clean Si(001)2 $\times$1 surface. It is known that the π band of the clean Si(001)2$\times$1 surface is dispersive along the Si dimer row (Γ-J' direction) but almost completely flat along the perpendicular dimer-row direction (Γ-J). This is a reflection of the fact that for the clean Si(001)2$\times$1 surface the interaction between dimers in the same row is substantially stronger than that between neighboring dimer rows. As we have seen, the observed uniform downward dispersion of the π surface band along both the J-Γ and J'-Γ symmetry directions for the Rb/Si(001) chemisorbed system is due to the lower rubidium adatoms chemisorbed at the valley bridge (C) sites. This would indicate that it is predominantly the lower rubidium adatoms [Rb(C)] of the Rb/Si(001) system which mediate the interaction between the Si dimers of the chemisorbed surface in both the Γ-J and Γ-J' directions.

The occupied electronic surface states denoted by the empty diamonds and asterisks in Fig. 2(c) represent the silicon dimer σ bond surface states, and the first silicon back bond states, respectively. Comparison with the surface states of the clean surface shows that the energy and dispersion of these two occupied surface states is little affected by the presence of the Rb adatoms on the surface. 3D charge density plots for the silicon dimer σ bond surface state at the J' point of the SBZ is plotted in Fig. 5(a). Comparing Figs. 2(b) and 2(c) along the Γ-J'_2 symmetric direction, it is apparent that both the first silicon back bond, and the silicon dimer σ bond, surface state bands correlate extremely well with the third (lowest energy) ARUPS surface state band reported by Chao *et al.*[30] Of these two surface states, however, only the silicon dimer σ bond surface state is not found near the Γ point of the SBZ, in agreement with experiment. This indicates that the C_3 surface state band determined by Chao *et al.*[30] is indeed the silicon dimer σ bond surface state, as they originally suggested. Plots of the $\rho_{nk}(z)$ function and charge density for the first silicon back bond surface state at the J point of the SBZ are presented in Fig. 5(b).

In addition to the occupied surface states, our calculations have also identified a number of unoccupied electronic surface states. These are indicated in Fig. 2(c) by the right and
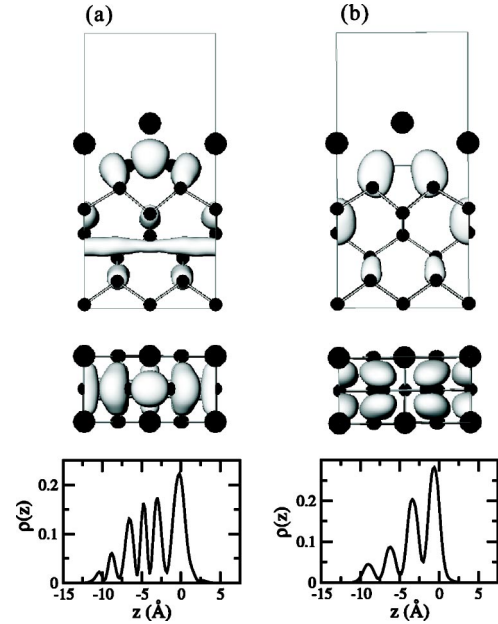

FIG. 5. Side and top views of the 3D charge density distributions, and the corresponding $\rho_{nk}(z)$, for the valence band surface states of the Si(001)2$\times$1-Rb system at 1.0 ML coverage indicated in Fig. 2(c) by (a) the empty diamonds and (b) the asterisks. The plots in (a) are for the J' point of the SBZ while those in (b) are for the J point. The charge density isosurface value for both plots was 0.8×10^{-2} e/Å^3.

left arrowheads, crosses, and solid diamonds. The low-lying unoccupied surface states result from the presence of the Rb adatoms. Due to the significant covalent character of the Rb-Si bonds, however, these states can be described as combinations of the Rb atomic orbitals and orbitals associated with the Si dimers. The states indicated by the right arrowheads in Fig. 2(c) are thus combinations of orbitals from the upper rubidium atoms [Rb(A)] and the π Si dimer dangling bond orbitals. 3D probability density plots for this unoccupied surface state at the J point of the SBZ, together with the corresponding $\rho_{nk}(z)$, are shown in Fig. 6(a). The dominant contribution to the probability density is observed to come from well above the silicon dimer atoms. 3D probability density plots for the unoccupied surface state at the J point of the SBZ represented by the left arrowhead in Fig. 2(c), are presented in Fig. 6(b). These unoccupied surface states are combinations of orbitals from the lower rubidium atoms and the π^* silicon dimer dangling bond orbitals. Again, the main contribution to the $\rho_{nk}(z)$ is seen to come from well above the surface. Analysis of the nature of these orbitals has shown that the contribution from the π Si dimer dangling bond orbitals to the lowest unoccupied surface state is very significant in the vicinity of the Γ point of the SBZ, but decreases steadily along the Γ-J-K and Γ-J' symmetric directions, to become negligible along the K-J' symmetric direction. The lowest unoccupied surface states which are represented by the crosses in Fig. 2(c) thus have little or no contribution from the Si dimer bonds, but have significant contributions from the upper rubidium and subsurface silicon
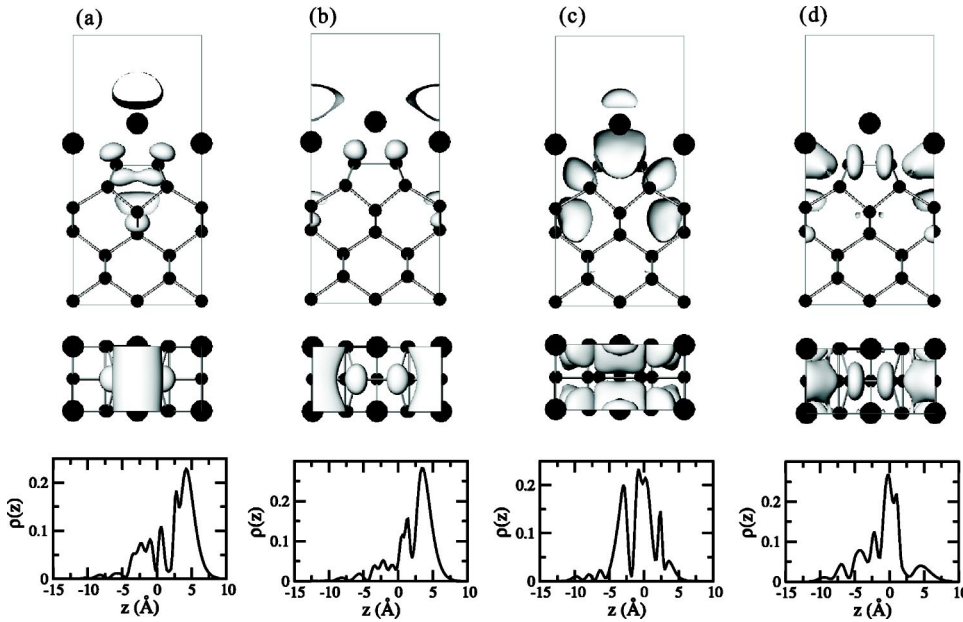
FIG. 6. Side and top views of the 3D probability density distributions, and the corresponding $\rho_{nk}(z)$, for the empty band surface states of the $Si(001)2 \times 1$-Rb system at 1.0 ML coverage indicated in Fig. 2(c) by (a) right arrowheads, (b) left arrowheads, (c) crosses, and (d) solid diamonds. The first two plots [(a) and (b)] are for the J point of the SBZ, while (c) and (d) are for the K-point and a wavevector between J and K, respectively. The probability density isosurface value was 1.06×10^{-2} Å^{-3} with the exception of (c) for which this value was 0.53×10^{-2} Å^{-3}.

atoms, as shown in Fig. 6(c). The final unoccupied surface states that we have identified are denoted in Fig. 2(c) by the solid diamonds. These are combinations of the atomic orbitals of the lower Rb atoms and the anti-bonding Si σ^* dimer bond molecular orbitals. 3D probability density plots for this surface state band for a wavevector along the J-K symmetry direction of the SBZ are given in Fig. 6(d).

The predicted dispersion of the low-lying unoccupied surface states is in excellent agreement with the parabolic-like dispersion of the IPES surface states obtained along the Γ-J and Γ-J' symmetric directions by Johannson *et al.*[31] [see Fig. 2(b)]. As stated earlier, this free-electron-like behavior led Johannson *et al.* to conclude that there must be strong Rb-Rb interactions within the overlayer. Our calculations, however, indicate that the low-lying states indicated by the right arrowheads in Fig. 2(c), which include mainly contributions from the upper rubidium, and the states denoted by the left arrowheads, which only involve the lower rubidium atoms, represent two essentially noninteracting, surface state bands. Analysis of these bands shows that they represent two distinct modes resulting from interactions between the Rb adatoms and the substrate, rather than between the Rb adatoms themselves. In Fig. 7 we have plotted the electronic structure of the isolated overlayer of the $Si(001)2 \times 1$-Rb chemisorption system and compared it with lowest-lying unoccupied surface state bands of the chemisorbed system. We observe, as expected, that the Rb-Rb interactions within the isolated overlayer result in a parabolic dispersion of the bands. The upper and lower Rb adatom-surface interactions in the $Si(001)$-Rb chemisorption system, however, are observed to be strong enough to drastically reduce the dispersion of the Rb-Rb "overlayer" bands along the Γ-J, J-K, and Γ-J' symmetry directions relative to that of the isolated Rb overlayer, and give rise to bands which are much less dispersive. Our calculations thus indicate strong interactions between the Rb adatoms and the substrate for the lowest unoccupied surface state bands, but provide little support for strong interactions between the rubidium atoms within the overlayer, as suggested by Johansson *et al.*[31]

IV. SUMMARY

In this paper we have investigated the atomic and electronic structure of the $Si(001)$-Rb system at 0.5 and 1.0 ML coverage using the plane wave pseudopotential DFT method contained in the VASP code. It has been found that at 0.5 ML coverage the atomic and electronic structures of the Rb chemsorption system are very similar to those of the Li chemisorption system. The minimum energy configuration of the $Si(001)2 \times 2$-Rb system at 0.5 ML corresponds to the two Rb adatoms in each 2×2 SUC occupying sites close to the pedestal and valley bridge sites. The predicted minimum energy structure for the $Si(001)2 \times 1$-Rb chemisorption system at 1.0 ML coverage has been found to be in good agreement with the XSW data, and the calculated electronic surface states shown to correlate extremely well with the ARUPS and IPES experimental results. The bonding between the Rb adatoms and the underlying Si substrate atoms has been determined to be neither ionic nor covalent. No evidence has been found for strong Rb-Rb interactions and the formation of a metallic overlayer.
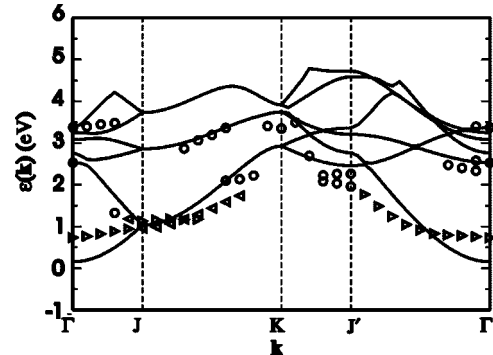

FIG. 7. The electronic band structure of the isolated Rb overlayer of the $Si(001)2 \times 1$-Rb chemisorption system at 1.0 ML coverage (full lines) compared to the low-lying unoccupied surface states of the chemisorbed system. The two sets of bands were moved to match at the J point of the surface brillouin zone.

*Corresponding author. Email address: Phil.Smith@newcastle.edu.au

[1] See articles, in *Physics and Chemistry of Alkali Metal Adsorption*, edited by H. P. Bonzel, A. M. Bradshaw, and G. Ertl (Elsevier, Amsterdam, 1989).

[2] *Metallization and Metal-Semiconductor Interfaces*, edited by I. P. Batra, NATO Advanced Study Institutes, Ser. B, Vol. 195 (Plenum, New York, 1989).

[3] R. I. G. Uhrberg and G. V. Hansson, CRC Crit. Rev. Solid State Mater. Sci. **17**(2), 133 (1991).

[4] J. D. Levine, Surf. Sci. **34**, 90 (1973).

[5] Y. Enta, T. Kinoshita, S. Suzuki, and S. Kono, Phys. Rev. B **36**, 9801 (1987); **39**, 1125 (1989).

[6] T. Abukawa and S. Kono, Phys. Rev. B **37**, 9097 (1988).

[7] Y. Morikawa, K. Kobayashi, K. Terakura, and S. Blügel, Phys. Rev. B **44**, 3459 (1991).

[8] T. Abukawa, T. Kashiwakura, T. Okane, Y. Sasaki, H. Takahashi, Y. Enta, S. Suzuki, S. Kono, S. Sato, T. Kinoshita, A. Kakizaki, T. Ishii, C. Y. Park, S. W. Yu, K. Sakamoto, and T. Sakamoto, Surf. Sci. **261**, 217 (1992).

[9] L. S. O. Johansson and B. Reihl, Phys. Rev. Lett. **67**, 2191 (1991).

[10] Y. Morikawa, K. Kobayashi, and K. Terakura, Surf. Sci. **283**, 377 (1993).

[11] K. Kobayashi, Y. Morikawa, K. Terakura, and S. Blügel, Phys. Rev. B **45**, 3469 (1992).

[12] P. Krüger and J. Pollmann, Appl. Phys. A: Solids Surf. **59**, 487 (1994).

[13] H. Q. Shi, M. W. Radny, and P. V. Smith, Phys. Rev. B **69**, 235328 (2004).

[14] H. Tochihara and Y. Murata, Surf. Sci. **215**, L323 (1989).

[15] L. S. O. Johansson and B. Reihl, Surf. Sci. **287/288**, 524 (1993).

[16] M. Eckhardt, H. Kleine, and D. Fick, Surf. Sci. **319**, 219 (1994).

[17] H. Kleine, M. Eckhardt, H. J. Jänsch, and D. Fick, Surf. Sci. **323**, 51 (1995).

[18] C. Y. Kim, K. S. Shin, K. D. Lee, and J. W. Chung, Surf. Sci. **324**, 8 (1995).

[19] L. S. O. Johansson, T. M. Grehk, S. M. Gray, M. Johansson, and A. S. Flodström, Nucl. Instrum. Methods Phys. Res. B **97**, 364 (1995).

[20] T. M. Grehk, L. S. O. Johansson, S. M. Gray, M. Johansson, and A. S. Flodström, Phys. Rev. B **52**, 16593 (1995).

[21] M. K.-J. Johansson, S. M. Gray, and L. S. O. Johansson, Phys. Rev. B **53**, 1362 (1996).

[22] K. D. Lee, C. Y. Kim, and J. W. Chung, Surf. Sci. **366**, L709 (1996).

[23] C. Y. Kim, H. W. Kim, J. W. Chung, K. S. An, C. Y. Park, A. Kimura, and A. Kakizaki, Appl. Phys. A: Mater. Sci. Process. **64**, 597 (1997).

[24] S. Hongo, S. Kaneko, and T. Urano, Surf. Sci. **433-435**, 775 (1999).

[25] K. Kobayashi, S. Blügel, H. Ishida, and K. Terakura, Surf. Sci. **242**, 349 (1991).

[26] P.-L. Cao, R.-H. Zhou, and X.-Y. Zhou, Phys. Lett. A **159**, 179 (1991).

[27] V. Eteläniemi, E. G. Michel, and G. Materlik, Surf. Sci. **251/252**, 483 (1991).

[28] Y.-C. Chao, L. S. O. Johansson, and R. I. G. Uhrberg, Appl. Phys. A: Mater. Sci. Process. **123/124**, 76 (1998).

[29] P. Castrucci, S. Lagomarsino, F. Scarinci, and G. E. Franklin, Phys. Rev. B **51**, 5043 (1995).

[30] Y.-C. Chao, L. S. O. Johansson, and R. I. G. Uhrberg, Phys. Rev. B **55**, 7667 (1997).

[31] L. S. O. Johansson, T. Dütemeyer, L. Duda, and B. Reihl, Phys. Rev. B **58**, 5001 (1998).

[32] G. Kresse and J. Hafner, Phys. Rev. B **47**, 558 (1993); **49**, 14251 (1994).

[33] G. Kresse and J. Furthmüller, Comput. Mater. Sci. **6**, 15 (1996).

[34] G. Kresse and J. Furthmüller, Phys. Rev. B **54**, 11169 (1996).

[35] G. Kresse and D. Joubert, Phys. Rev. B **59**, 1758 (1999).

[36] P. E. Blöchl, Phys. Rev. B **50**, 17953 (1994).

[37] D. Vanderbilt, Phys. Rev. B **32**, 8412 (1985).

[38] C. A. Coulson, L. R. Redei, and D. Stocker, Proc. R. Soc. London **270**, 357 (1962).